IN-09
49573

NASA TECHNICAL MEMORANDUM

NASA TM-88482

38P

SHOCK WAVE/TURBULENT BOUNDARY LAYER INTERACTION IN THE FLOW FIELD OF A TRIDIMENSIONAL WIND TUNNEL

R. Benay and T. Pot

Translation of: "Interaction onde de choc/couche limite turbulente en ecoulement de canal tridimensionnel," ONERA, TP, No. 1985-151, 1985

(NASA-TM-88482) SHOCK WAVE/TURBULENT BOUNDARY LAYER INTERACTION IN THE FLOW FIELD OF A TRI-DIMENSION WIND TUNNEL (National Aeronautics and Space Administration) 38 p CSCL 14B G3/09

N87-15980

Unclas 43176

NATIONAL AERONAUTICS AND SPACE ADMINISTRATION
WASHINGTON, D.C. 20546 SEPTEMBER 1986

ORIGINAL PAGE IS
OF POOR QUALITY

STANDARD TITLE PAGE

1. Report No. NASA TM-88482	2. Government Accession No.	3. Recipient's Catalog No.
4. Title and Subtitle SHOCK WAVE/TURBULENT BOUNDARY LAYER INTERACTION IN THE FLOW FIELD OF A TRI-DIMENSION WIND TUNNEL		5. Report Date 6. Performing Organization Code
7. Author(s) R. Benay and T. Pot		8. Performing Organization Report No. 10. Work Unit No.
9. Performing Organization Name and Address SCITRAN Box 5456 Santa Barbara, CA 93108		11. Contract or Grant No. NASw- 4004 13. Type of Report and Period Covered Translation
12. Sponsoring Agency Name and Address National Aeronautics and Space Administration Washington, D.C. 20546		14. Sponsoring Agency Code

15. Supplementary Notes
Translation of: "Interaction onde de choc/couche limite turbulente en coulement de canal tridimensionnel," ONERA, TP, No. 1985-151, 1985

16. Abstract
This paper presents the first results of a thorough experimental analysis of a strong 3D shock-wave/turbulent boundary-layer interaction occurring in a three-dimensional transonic channel. The aim of this experiment is to help in the physical understanding fo a complex field, including several separations, and to provide a well documented case to test computational methods. The flowfield has been probed in many points by means of a three-component Laser Doppler Velocimeter. The results here presented are only relative to the mean velocity field. They clearly show the formation in the flow of a strong vortical motino resulting from the shock wave interaction.

17. Key Words (Selected by Author(s))	18. Distribution Statement Unclassified and Unlimited		
19. Security Classif. (of this report) Unclassified	20. Security Classif. (of this page) Unclassified	21. No. of Pages 38	22. Price

TM 88482

SHOCK WAVE/TURBULENT BOUNDARY LAYER INTERACTION IN THE FLOW FIELD OF A TRIDIMENSIONAL WIND TUNNEL

by BENAY, R and POT T.

22d Symposium on Applied Aerodynamics
Lille, 13-15 November 1985

NATIONAL CENTER FOR AEROSPACE TEST AND RESEARCH
29 Avenue de la Division Leclerc--92320 CHATILLON

AAAF Symposium--November 1985

SHOCK WAVE/TURBULENT BOUNDARY LAYER INTERACTION IN THE FLOW FIELD OF A TRIDIMENSIONAL WIND TUNNEL

by

R. BENAY and T. POT

National Center for Aerospace Test and Research
B.P. 72 92322 CHATILLON CEDEX

SUMMARY -

This paper presents the first results of a thorough experimental analysis of a strong 3D shock-wave/turbulent boundary-layer interaction occurring in a three dimensional transonic channel. The aim of this experiment is to help in the physical understanding of a complex field, including several separations, and to provide a well documented case to test computational methods. The flowfield has been probed in many points by means of a three-component Laser Doppler Velocimeter. The results here presented are only relative to the mean velocity field. They clearly show the formation in the flow of a strong vortical motion resulting from the shock wave interaction.

/3/

CONTENTS

1. INTRODUCTION

The phenomena referred to as the interaction between shock wave and boundary layer, most frequently turbulent, play, as is known, a very important role in numerous devices in use: transsonic airfoils, helicopter blades, turbomachinery, supersonic airscoops, propulsive nozzles etc. Their effects are mostly harmful, particularly if the interaction causes a boundary layer separation. It can then result in considerable loss in performance (a heavy loss of lift, a brisk increase in drag, drop in efficiency etc.), with the almost concomitant appearance of large scale stagnations which are extremely injurious (stall, vibrations, etc.).

From this comes the very important research effort dedicated to shock/boundary layer interaction with the objective of better understanding the physics of these phenomena, to model them correctly and to develop control techniques making it possible to prevent their negative consequences (1).

Without entering further into an exhaustive examination of the shock/boundary layer interaction (the interested reader can turn to the references (2, 3, 4) for much more complete data), attention is drawn to the fact that very substantial progress has been accomplished in recent years in experimental analysis, and especially in modeling these phenomena in bidimensional flow, whether by using methods of perfect fluid/viscous fluid coupling (5, 6, 7), or by solution of the comprehensive Navier-Stokes equations averaged in time (8, 9, 10). However, in the most current practice, except for those devices with symmetry of revolution (e.g. propulsive nozzles), the flows are very generally tridimensional. The interaction problem becomes then much more complex and more a question of the understanding of the physics than of the theoretical forecasting; the knowledge and the available results are still fragmentary (in references (4)

and (11) one will find a summary of the studies carried out in the tridimensional).

Also, the object of the experimental testing, the first results of which are presented here, is to furnish a well documented and detailed set of data on the shock wave/turbulent boundary layer interaction generated in the tridimensional wind tunnel. The data thus obtained can be utilized to help in understanding the complex interactive flows and to evaluate the computational methods and the turbulence modelling.

This study is an extension to tridimensional flows of numerous investigations already carried out at ONERA on flows in the bidimensional transsonic tunnel. (12)

The tests, the results of which have been commented on below, were based on very wide use of the three-component laser doppler velocimeter. This is, as far as we know, the first time that there have been published such detailed measurements carried out, thanks to this technique, in very high velocity tridimensional flow.

2. EXPERIMENTAL APPARATUS AND MEASUREMENT TECHNIQUES /5/

2.1--Test Setup--Definition of the Wind Tunnel

The photo in Figure 1 gives an overall view of the experimental apparatus. This consists essentially of a subsonic/supersonic test cell of which the upper wall is flat and the lower wall has a "hump", the two lateral faces being constituted of flat glass. The span of the test cell is 120mm and its height, at the entrance section, is 120mm. The hump (see Figure 2) has upstream a rectilinear part, the slope of which relative to the horizontal is 7° This first part, which practically gives the tunnel a bidimensional form, is followed by an evolving contour, at first circular convex, then circular concave, the two arcs of the circle being defined in a way to assure continuity of the slopes at their junction point as well as their contacts with the rectilinear parts upstream and

downstream. The tridimensional effect is obtained by giving to the line along the summit of the hump an inclination of 60^{o} with respect to the upstream flow. Downstream of the summit line, the generation of the form is cylindrical.

The subsonic flow coming from upstream is accelerated in the convergent section of the test cell so as to attain the sonic state in the vicinity of the hump which constitutes a neck. Downstream, the flow becomes supersonic; then, due to the deflection imposed by the form of the lower wall it is the center of compressions giving birth to the shock waves interacting vigorously with the boundary layers which are generated on the four sides of the test section.

Downstream of the test zone, there is disposed a second neck with a regulated opening (not represented in Figure 2) which, when put into operation, makes it possible to isolate from the flow under study those acoustic perturbations causing canalizations which could become a source of parasitic instabilities.

The shape of the tunnel has been defined taking care to facilitate its description using computational methods by avoiding, in particular, excessively abrupt gradients in the discontinuities or variations which frequently give rise to difficulties in linkage.

On the other hand, as we will see, the transsonic flow thus generated is strongly tridimensional and is much more complex than those studied heretofore which are generally supersonic (13, 14, 15).

2.2 Measurement Techniques

The upper and lower walls of the test cell are each equipped with 250 static pressure openings. The parietal flows on the four sides of the tunnel have been examined from spectra obtained by the viscous layer technique. The measurements of the field based at the same time on the mean and fluctuating characteristics have been carried out with the help of a three-component laser doppler

velocimeter; we will briefly describe its characteristics and mode of functioning adopted for these tests.

The apparatus, the block diagram of which is shown in Figure 3, has been developed by the General Physics Directorate of ONERA, in cooperation with the Laser Metrology Group of the Aerodynamics Directorate (for more detail, see reference (16)). /6/

The velocimeter is equipped with two emitting sources consisting of two identical argon lasers capable of emitting at all wave lengths a beam power of 15W. The first functions with a violet monoray (wave length $\lambda = 0.4765\,\mu m$) at a power 3W. The second is used at all wavelengths at less than 6W, and its beam is divided into two colors by dichroic semi-transparent plates: green ($\lambda = 0.5145\,\mu m$) and blue ($\lambda = 0.488\,\mu m$). The blue pencil beam, the wave length of which is very close to violet, is refined by a prism to suppress the parasite frequencies which the dichroic plate will have allowed to pass through. The three pairs of pencil beams which result by the traversing of three dividers (D_{Vi}, D_B, D_{Ve}) are focussed to make up the measurement space, of which the diameter used is about 400 μm. In the present configuration, the blue and green rays are emitted in a horizontal plane conforming to a direction inclined 25.17^o to the axis OY following the span of the assembly (see Figure 2). Their interference produces two fringe systems, one horizontal, the blue, and the other vertical, the green, contained in a plane perpendicular to the direction of emission. The violet ray is also emitted in a horizontal plane along a direction inclined 23.33^o to the OY axis. It produces a network of vertical fringes in a plane perpendicular to this direction.

Therefore, the velocity vector is measured in a system of axes, of which one is vertical, OZ, and the other two OX_1 and OX_2, contained in a horizontal plane forming an angle of 48.5^o to each other. Simple formulae enable expression of the velocity vector components in the assumed system of axes OX, OY, OZ (see Figure 2).

The adjustments used lead to the following values for the interference fringes: 37.34 μm for the blue, 38.61 μm for the green, and 35.93 μm for the violet.

In order to allow the system to detect the orientation of the velocity component measured, the six pencil beams going through the Bragg cells induce a breakup of the fringes in the interior of the measurement space where the frequency of the modulation is 7.5 MHz for the blue and violet and 10 MHz for the green.

The reception unit consists of two Cassegrain telescopes of 200mm opening so as to collect a maximum of the radiation diffused by the particles traversing the measurement space. The first is mounted with interferential filters which allow extraction and separation of the green and blue rays in the light which it receives. The second telescope selects the violet in the same way. The rays thus separated are then sent to a photomultiplier. The signals which they deliver are entered into the DISA-55L computer, the digital outputs of which are connected to an acquisition system through the intermediary of a simultaneous digitalizer. This apparatus allows assurance that the three velocity measurements carried out are indeed related to the same particle which just traversed the measurement space. The window of this digitalizer is here set at 1 μsec.

The system can function either in forward diffusion or retrodiffusion. In the present tests, the mode of forward diffusion has been adopted, which produces a much larger signal-to-noise ratio. Therefore, the emission and reception assemblies are mounted on two movable tables of precise displacement (uncertainty of 0.05mm) conforming to three perpendicular directions. They are guided by a computer which coordinates their movements such that the optical collector follows the measurement space in the course of its displacement. /7/

In order to obtain an adequate acquisition rate, especially in the turbulent regions, the flow was injected with smoke

emitted from a cannister located in the plenum of the blower.

At each measurement point there took place the recording of three components of the instantaneous velocity by a sampling of 2000 events corresponding to the traversing of the measurement space by 2000 particles (that is a total: 3 x 2000 = 6000 instantaneous values for the u, v, w, components along OX, OY, OZ respectively). The HP2100S computer associated with the velocimeter makes it possible to obtain, with slight delay, the most common statistical terms; that is for two fluctuating variables x and y:

- the mean value: $\overline{x} = \frac{1}{N}\sum_{i=1}^{N} x_i$; $\overline{y} = \frac{1}{N}\sum_{i=1}^{N} y_i$; $\overline{z} = \frac{1}{N}\sum_{i=1}^{N} z_i$
- the standard deviation: $\sigma_x = \left[\frac{1}{N-1}\sum_{i=1}^{N}(x_i - \overline{x})\right]^{1/2}$; $\sigma_y \ldots$
- the correlation: $\overline{xy} = \frac{1}{N}\sum_{i=1}^{N}(x_i - \overline{x})(y_i - \overline{y})$

The magnitudes such as $\sigma'x^2$ and $\overline{xy}$ are identified as components of the Reynolds tensor. The set of results is also stored on magnetic tape in order to be able to exploit them more completely on a high powered computer.

3. PRESENTATION OF THE RESULTS

3.1 Visualization of the parietal flow

The parietal spectra obtained by viscous layer technique constitute a valuable and almost indispensable aid in the understanding of the structure of tridimensional flows, particularly when separations are produced. The layer lines observed can, with a good degree of confidence, be in effect compared to the parietal flow currents of the actual flow field. These lines are defined as the limit, when the distance to the wall approaches zero, of the lines of current, and these are identified with the lines of friction, which are the force lines of the vector field set up by the parietal friction. It is the close examination of the topology of the friction lines, and more

especially the observation of singularities (centers, nodes, necks) revealed by their network, which permits a more certain definition of the separation in tridimensional flow, where this concept is far from being as clear even as in the case of the bidimensional (17, 18).

Figures 4, 5 and 6 show photographs of parietal spectra /8/ observed on the hump and on the lateral faces A and B of the test section (see Figure 2). Figure 4, related to the surface of the hump reveals a practically bidimensional upstream flow where the parietal lines are parallel to the longitudinal axis OX. Especially in the vicinity of face A, the flow is rapidly deflected by a shock which is generated a little downstream of the summit of the hump. The measurements in the field (see more below), confirm by the increase of parietal pressure, that the maximum Mach number on the side upstream of this shock is about 1.65. At the base of the shock a strong interaction with the boundary layer appears accompanied by the formation of a very complex structure. The parietal friction lines show the existence of a first separation line getting underway near face B of the test section. This line, in actuality, separates two sets of friction lines: for the one near B, the latter are relatively little deviated and propagate in a continuous manner from upsteam towards downstream; in the other case, the friction lines curve inward distinctly in the direction of face A and then flow back towards upstream, where, with the lines coming from the summit of the hump, they roll around a center which is the trace on the wall of a turbulence slipping out from the external flow. A second line of separation can exist very close to A, but the visualization is not sufficiently discriminating to give clear evidence of this.

Figure 5 shows the spectrum on vertical face A. One observes right away very clearly in the region closest to the hump a quasi-discontinuity in the network of parietal friction lines which envelop a separation line S_1, characteristic of a strong

interaction by lateral shock (glancing or skewed shock-wave).

More downstream, the parietal lines seem to go up again from the lower wall showing the creation of a strong ascendant current induced by a turbulence very close to A.

These lines envelop a second line of separation S, at least a line of attachment being obliged to exist between S_1 and S_2. However, due to the weak velocities which prevail, the parietal spectrum in this region is not sufficiently clear because the structure of flow can no longer be precisely stated. Other visualizations will be needed to clarify this point.

The upper part of the photograph shows a large structure formed by the rolling-up of the friction lines around a center which is at the origin of a turbulence.

On face B (see Figure 6), the parietal spectrum is markedly less complex. No line of separation is discernible in the vicinity of the hump where the deflection of the friction lines downstream of the summit results in a relatively less intense lateral shock. On the other hand, near the upper wall a center forms. All of these observations tend to show that the interaction on the upper wall, and correlatively on the upper part of lateral faces A and B, is much stronger than on the hump. In fact, the oblique shock being created in the proximity of the hump tends to become normal near the upper wall, causing a clearly more intense interaction. This tendancy is confirmed by the field measurement which we will now present.

3.2 Field Measurements /9/

The cross-hatched area in Figure 2 shows the projection on the surface of the hump of the regime investigated with the laser velocimeter. The volume analyzed has been sampled along 75 vertical stations each comprising 50 measurement points, that is a total of 3750 points to define the flow in the sector located downstream of the summit of the hump where the interaction phenomena are assumed to be the most intense.

The results presented here will only be concerned with the

mean flow, since the turbulence measurements, where the interpretation is more sensitive, are still being studied.

In the first place we will examine the field in the form of projections of the velocity vectors in the longitudinal planes XZ, numbered from 1 to 5 in Figure 2. We begin at plane 5 which is the closest to face B (it is situated at a transverse distance Y - 90mm from A). The plot of Figure 7, where in the interest of clarity the scale along Z has been strongly compressed (the same is noted for Figures 8, 9, 12 and 13), demonstrates the following characteristics:

- The flow is the site of an oblique shock wave the passage of which in the vector field is barely visible;
- In contact with the wall there develops a boundary layer the thickness of which is small during the interaction.

In planes 4 and 3 (Y = 75mm and Y = 60mm, see Figures 8 and 9),the longitudinal field has a very close organization. The structure of the flow is better visualized by the traces of the iso-Mach lines of these planes represented in Figures 10 and 11. One will observe very plainly, especially in plane 4, a structure of shocks in lambda comprising a shock with oblique top C_1 (its zigzag course is caused by imperfections in the interpolation/smoothing program used to compute the iso curves), followed by a quasi-normal shock C_2. The mach number Mo on the wall upstream of C_1 is about 1.45; downstream it is clearly 1.1; with the result that C_2 is very much less intense. In the section downstream of the tunnel, the Mach number is unity. Shocks C_1 and C_2 converge at a triple point situated at the limit of the regime investigated. It is to be noted that in smooth transonic flow a structure of this kind is generally associated with a major separation of the boundary layer, with return current, a phenomenon which was not observed here. In fact in tridimensional, the flow has a transverse component which causes the Mach number Mn normal to the shock to be markedly lower than Mo; but it is Mn which is drives the appearance of the separation

which takes place at Mn $\cong$ 1.3 (19).

In addition, in tridimensional, the flow has the possibility of slipping out transversely when it is submitted to an antagonistic pressure gradient, hence the separation can not be accompanied by a spectacular thickening of the boundary layer as in bidimensional.

When one comes close to face A (planes 2 and 1, see Figures 12 and 13), a considerable change in the structure of the field is produced. Close to the hump, the longitudinal velocity /10/
profiles present, for plane 2, a deficiency zone which develops from X = 280mm. This minimum is situated at an appreciable distance from the wall. Upon approaching the wall, the longitudinal velocity grows and one subsequently observes again a profile of the classical boundary limit. Downstream, the velocity trough spreads vertically until it disappears little by little. In plane 1, situated at 30mm from wall A (see Figure 13), the phenomenon is accentuated and between X = 290mm and X = 310mm, the longitudinal velocity becomes extremely weak on an appreciable vertical extension going up to the wall.

The subsequent figures represent the projections of the vector velocities in transverse plane ZY.

The first result (see Figure 14) is situated at X = 260mm relative to plane 6, that is to say it correponds to the velocity field immediately downstream of the shock. In a general way, and under the influence of the hump, the transverse flow at this station goes from face A towards face B and shows a prolonged component. Equally, it is noted that the component of the transverse velocity is much larger near the hump than in the external zone of the field.

From X = 270mm (plane 7 in Figure 2), there is produced a large change in the structure of the transverse field. At station Y = 45mm (that is, in the half of the tunnel closest to face A), the vector velocity (transverse) rotates rapidly in the immediate proximity to the hump where it is directed from B towards A.

Further downstream (see Figures 16 and 17), this movement is amplified. It shows the development in the middle of the flow of a turbulence with an obviously longitudinal axis, the curve of which on the wall is shown by the visualization in Figure 4. This turbulence, actually very flattened, is more clearly shown by the curve of the iso-module lines of velocity in Figure 18. The vector fields in Figures 16 and 17 also show the discontinuity of the transverse component at the passage of the shock wave which is formed in the tunnel.

When one then moves further downstream (see Figures 19 to 21), the rotational movement remains visible and seems to have to more and more involve a part of the flow. At the same time, one witnesses a general diminution of the amplitude of the transverse component, especially detectible in the section furthest in the field exterior and in the regions closest to wall B.

This tendency shows the alignment of the whole of the flow along the longitudinal axis of the tunnel the section of which becomes constant again.

4. CONCLUSION

The flow resulting from an interaction of shock wave/turbulent boundary layer being propagated in a transsonic tunnel of tridimensional geometry has been investigated in detail with a three-component laser doppler velocimeter. These measurements, complemented by parietal visualizations with viscous layers, make possible definition of the structure of the complex tridimensional field, characterized by the existence of wide separations. In particular, one notes downstream of the shock originating on the lower evolutive wall of the tunnel /11/ the formation of a turbulence, the axis of which tends to align itself rapidly in the principal direction of the flow. This phenomenon seems to border on that observed on swept wings in transsonic. The present tests should therefore make possible better comprehension of the physics of these interactions and they could also serve to validate the computational methods under

development by producing a complete experimental data set.

However, more extended study will be necessary to get from results already available a truly clear image of a flow, the structure of which is extremely complicated. Otherwise, the laser velocimeter has also furnished numerous data on the fluctuating characteristics of the field; their study, currently underway, will give valuable indications to help in modelling the turbulence.

REFERENCES

1 - DELERY, J. "L'interaction onde de choc-couche limite turbulente et son contrôle." AGARD-CP n°365, Paper 21 (1984) et ONERA TP n°1984-27.

2 - LEBLANC, R. "Recent Progress in Shock-Wave/Boundary Layer Interaction." VKI, LS-84 on "Transonic Blade to Blade Flow in Axial Turbomachinery" (Fev.1976).

3 - STANEWSKY, E. "Wechselwirkung Zwischen Aussenstromung und Grenzchicht an transsonischen Profilen." Thèse de Docteur-Ingénieur, D-83, Berlin (Mai 1981).

4 - DELERY, J. et MARVIN, J.G. "Turbulent Shock-Wave/Boundary-Layer Interaction." AGARDograph n°280 (en cours d'édition).

5 - LE BALLEUR, J.C. et BLAISE, D. "Calculs des écoulements internes décollés et de l'interaction couche limite-onde de choc par couplage visqueux-non visqueux." La Recherche Aérospatiale, n°1985-4.

6 - MEAUZE, G. et DELERY, J. "Méthode de couplage pour le calcul en mode inverse des écoulements internes transsoniques avec onde de choc." AGARD-CP n°351 et ONERA TP n°1983-62.

7 - WHITFIELD, D.L. et THOMAS, J.L. "Transonic Viscous Invicid Interactions Using Euler and Inverse Boundary-Layer Equations." Computational Methods in Viscous Flows in Recent Advances in Numerical Methods in Fluids, W.G. Habashi, Editor, Pineridge Press (1983).

8 - ESCANDE, B. et CAMBIER, L. "Turbulence Modeling in Transonic Interactions." IUTAM Symposium on "Turbulent Shear-Layer/Shock-Wave Interactions, 9-12 Septembre 1985, Palaiseau, France-Springer-Verlag (à paraître en 1986).

9 - VANDROMME, D. et HA MINH H. "Physical Analysis of Turbulent Boundary Layer/Shock-Wave Interactions Using Second Order Closure Predictions." IUTAM Symposium on "Turbulent Shear Layer/Shock Wave Interactions, 9-12 Septembre 1985, Palaiseau, France-Springer-Verlag (à paraître en 1986).

10 - JOHNSON, D.A. et KING, L.S. "A New Turbulence Closure Model for Boundary Layer Flow with Strong Adverse Pressure Gradients and Separation." AIAA Paper n°84-0175.

11 - PEAKE, D.J. et TOBAK, M. "Three-Dimensional Interactions and Vortical Flows with Emphasis on High Speeds." AGARDograph 252 (juillet 1980).

12 - DELERY, J. "Experimental Investigation of Turbulent Properties in Transonic Shock/Boundary Layer Interactions." AIAA Journal, Vol.21, n°2, pp.180-185 (Fév. 1983) ; voir aussi AIAA Paper n°81-185 (Juin 1981).

13 - OSKAM, B., VAS, I.E. et BOGDONOFF, S.M. "Mach 3 Oblique Shock-Wave/Turbulent Boundary Layer Interactions in Three Dimensions." AIAA Paper n°76-336 (Juillet 1976).

14 - SETTLES, G.S., PERKINS,J.J. et BOGDONOFF, S.M. "Investigation of Three Dimensional Shock/Boundary-Layer Interactions at Swept Compression Corners." AIAA Journal, vol.18, n°7 (Juillet 1980). /13/

15 - KUSSOY, M.I., VIEGAS, J.R. et HORSTMAN, G.C. "An Experimental and Numerical Investigation of a 3D Shock Separated Turbulent Boundary-Layer." AIAA Journal, vol.18, n°12 (Décembre 1980).

16 - BOUTIER, A., D'HUMIERES, C. et SOULEVANT, D. "Three Dimensional Laser Velocimetry : a Review." 2nd International Symposium on Application of Laser Anemometry to Fluid Mechanics, Lisbone, 2-5 Juillet 1984 et ONERA TP 1984-43.

17 - LEGENDRE, R. "Lignes de courant d'un écoulement permanent. Décollement et Séparation." La Recherche Aérospatiale n°1977-6.

18 - LIGHTHILL, M.J. "Attachment and Separation in Three-Dimensional Flows." Section II 2-6 of Laminar Boundary Layers, Oxford University Press (1963), pp. 72-82.

19 - MIGNOSI, A. DOR, J.-B. et SERAUDIE, A. "Experiemntal Study of the Boundary Layer Separation Conditions throught a Shock-Wave on Airfoils and Swept Wing." IUTAM Symposium on "Turbulent Shear-Layer/Shock-Wave Interactions, 9-12 Septembre 1985, Palaiseau, France-Springer-Verlag (à paraître en 1986).

REFERENCES REQUIRING TRANSLATION:

1 DELERY, J. "The shock wave/turbulent boundary layer and its testing" AGARD-CP No. 365, Paper 21 (1984) and ONERA TP No 1984-27.

3 STANEWSKY, E. "Reaction between parasitic flow and boundary layer on transsonic profiles" Thesis for Dr.-Ing., D-83, Berlin,(Mayl981)

5 LE BALLEUR, J.C. and BLAISE D. "Computation of separated internal flows and of the boundary layer/shock wave interaction by viscous/non-viscous coupling" La Recherche Aerospatiale, No. 1985-4

6 MEAUZE, G. and DELERY, J.: "Coupling method for the computation in inverse mode of internal transsonic flows with shock wave" AGARD-CP No. 351 and ONERA TP No 1983-62

17 LEGENDRE, R. "Current lines of a standing flow. Separation and splitting" La Recherche Aerospatiale No. 1977-6

ORIGINAL PAGE IS
OF POOR QUALITY

/14/

Figure 1: Photo of the experimental apparatus

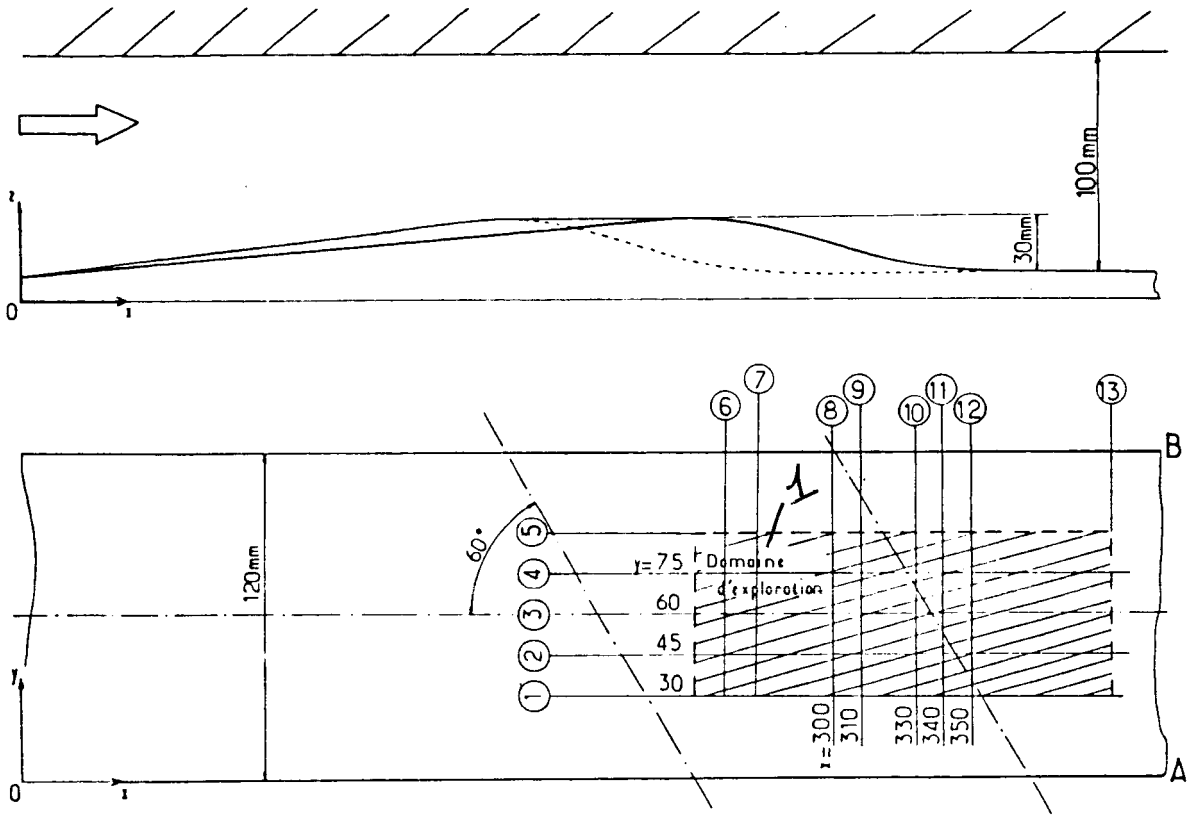

Figure 2: Definition of the regime of the study

1. study regime

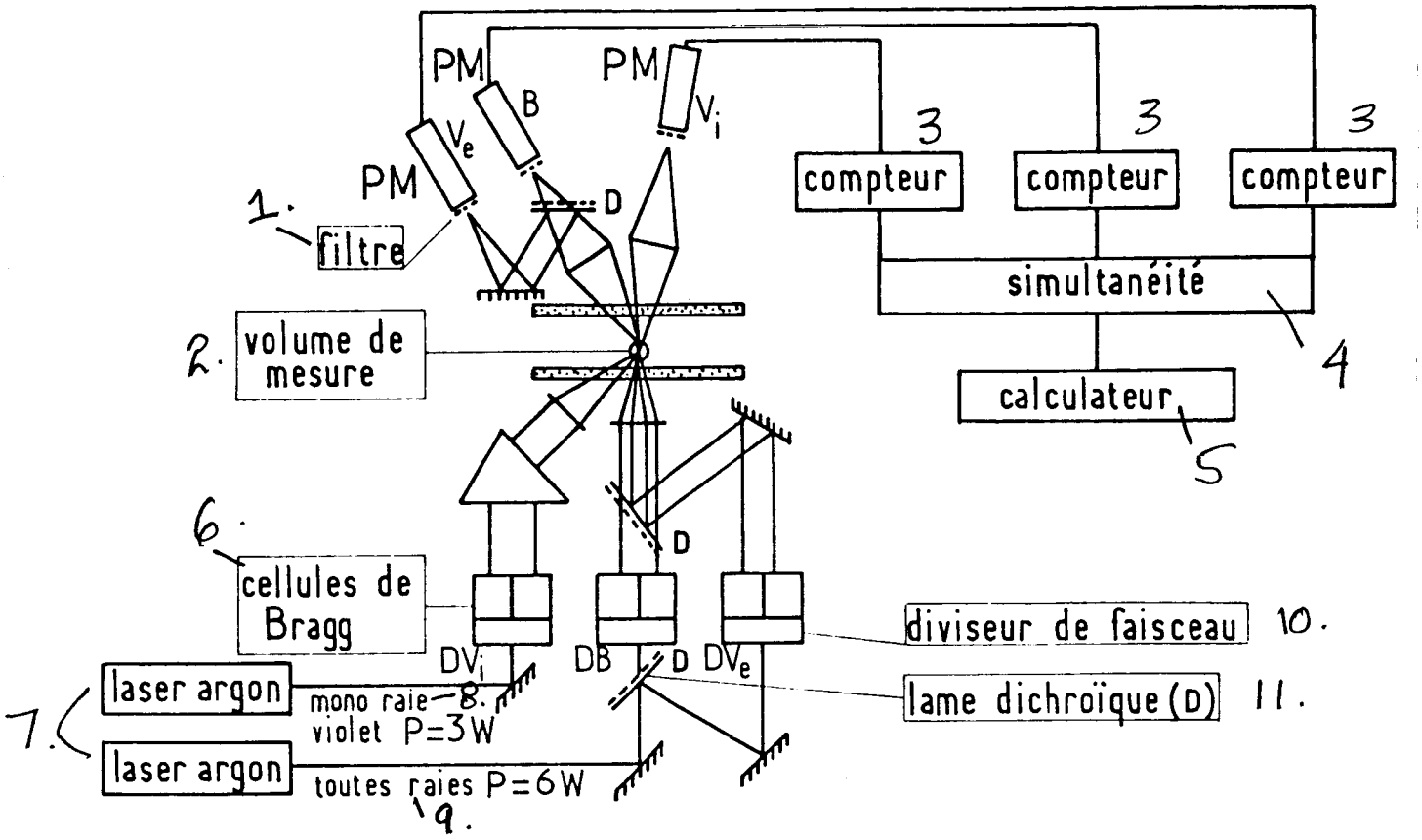

Figure 3: Block diagram of the three-component laser doppler velocimeter

1. filter
2. measurement space
3. counter
4. overlap
5. computer
6. Bragg cells
7. argon laser
8. monoray
9. all rays
10. beam divider
11. dichroic plate

ORIGINAL PAGE IS
OF POOR QUALITY

Figure 4: Visualization at the wall on the hump

ORIGINAL PAGE IS
OF POOR QUALITY

Figure 5: Visualization at the wall on face A

Figure 6: Visualization at the wall on face B

ORIGINAL PAGE IS
OF POOR QUALITY

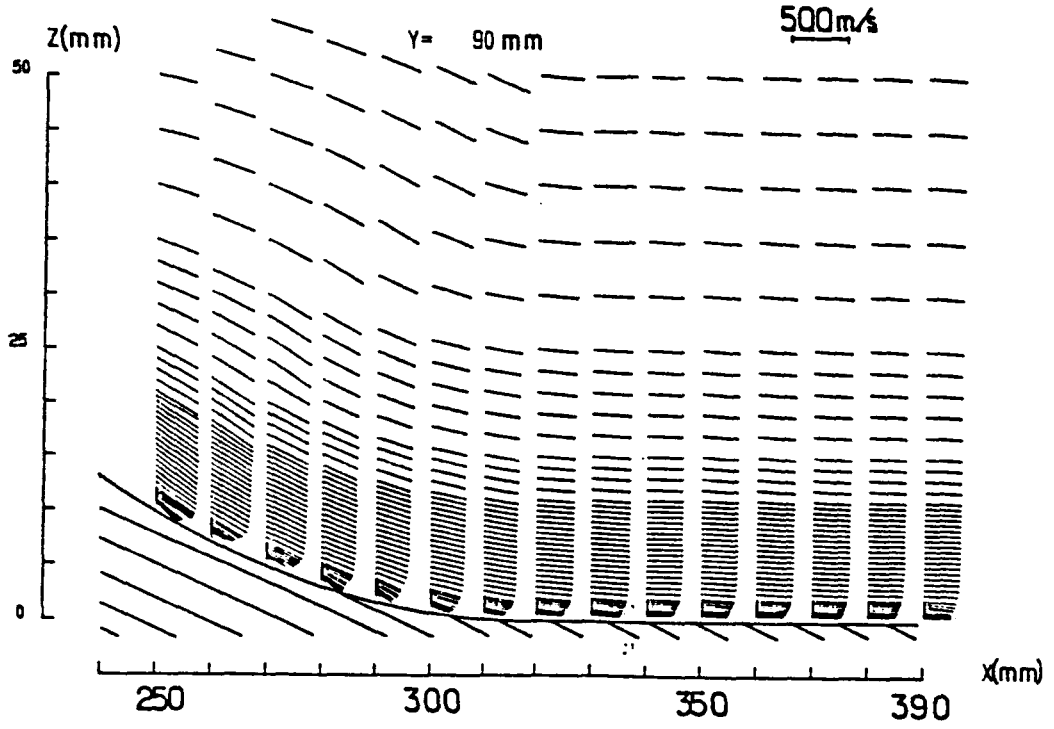

Figure 7: Projection of the velocity vectors in the longitudinal plane 5

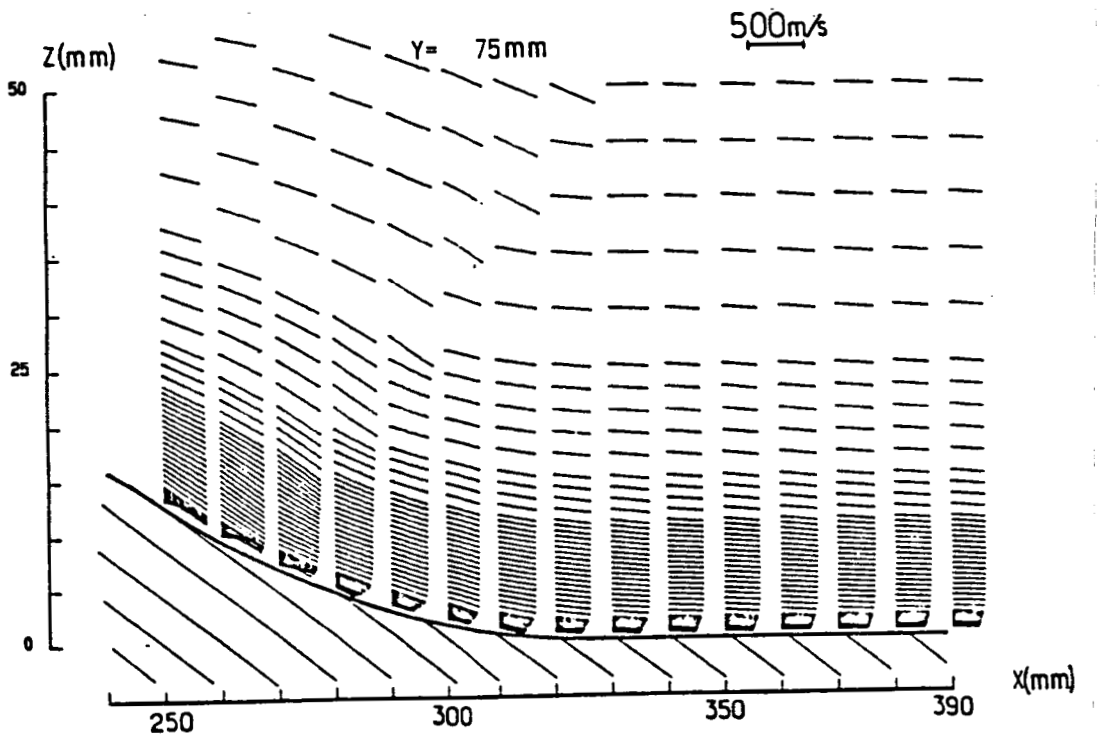

Figure 8: Projection of the velocity vectors in the longitudinal plane 4

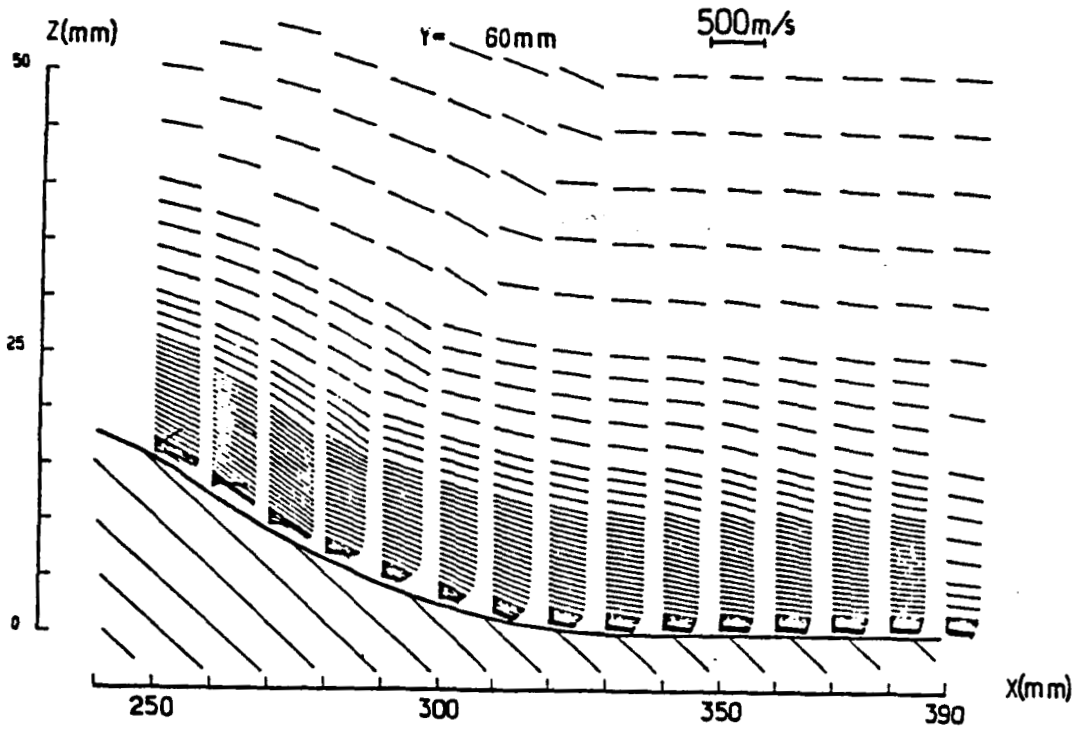

Figure 9: Projection of the velocity vectors in the longitudinal plane 3

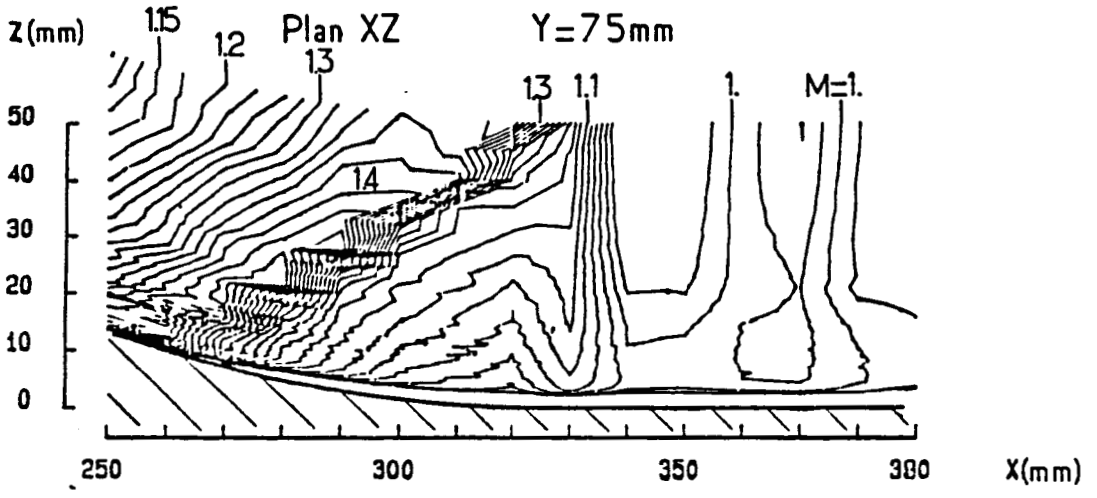

Figure 10: Iso-Mach lines in longitudinal plane 4

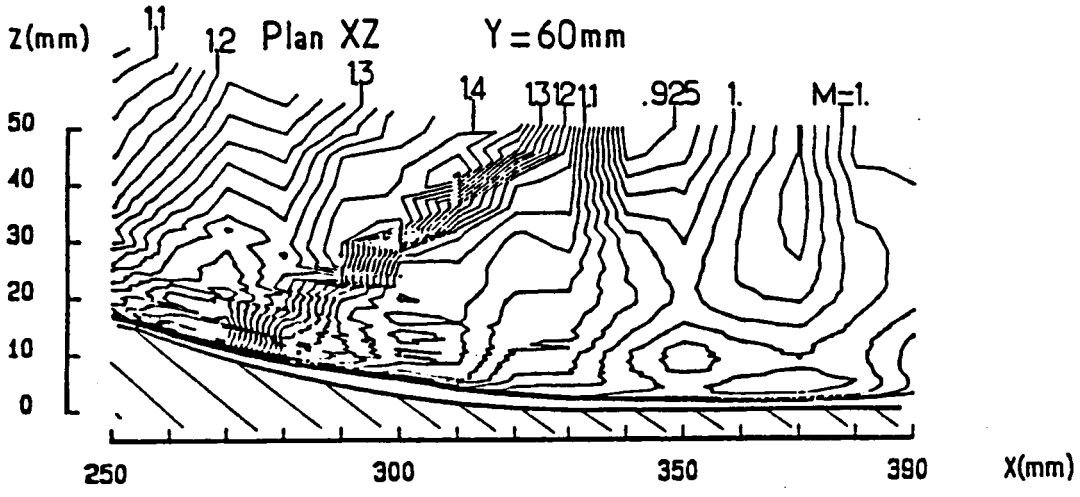

Figure 11: Iso-Mach lines in longitudinal plane 3

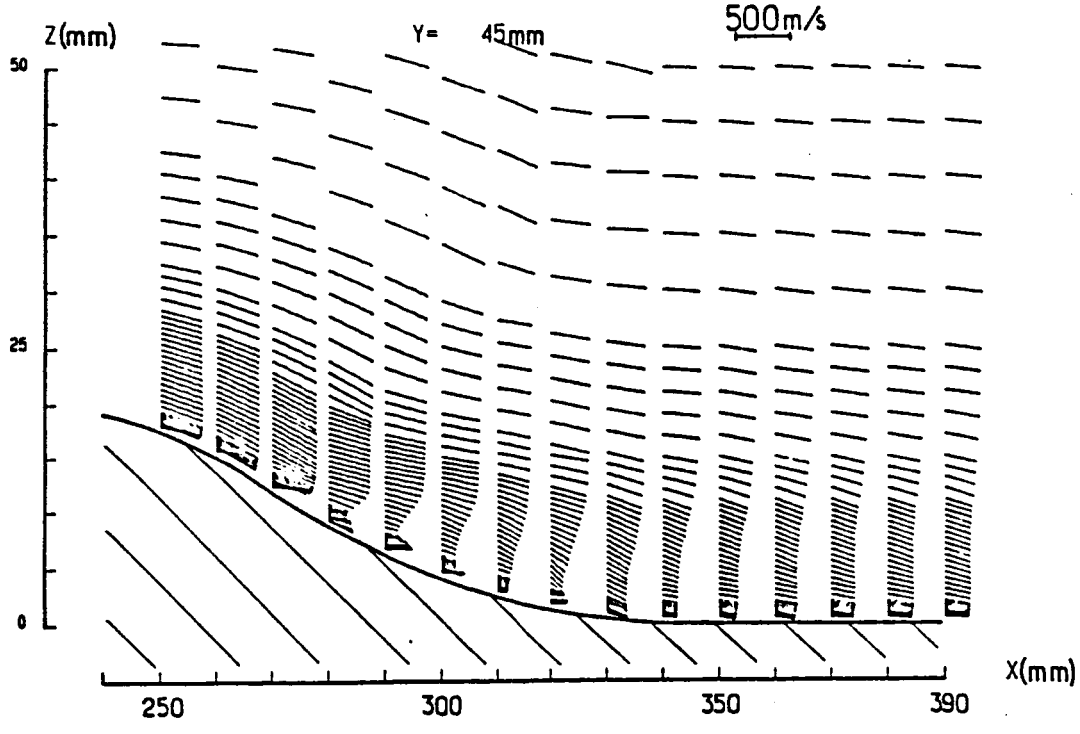

Fig.12: Projection of the velocity vectors in the longitudinal plane 2

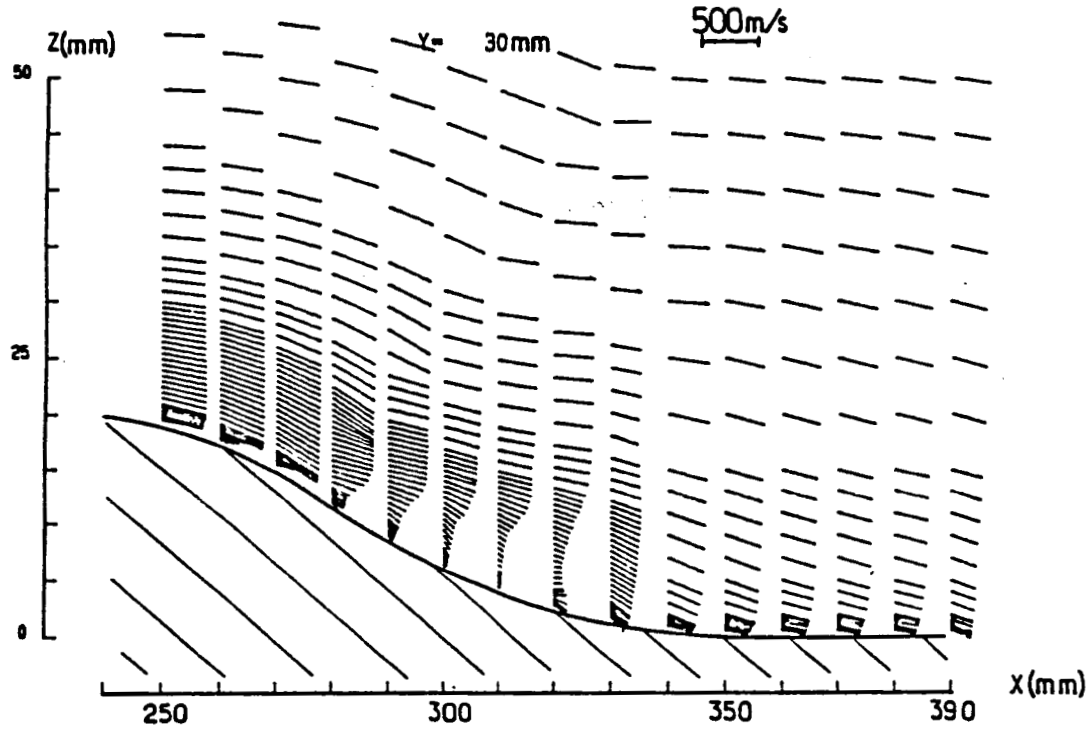

Fig. 13: Projection of the velocity vectors in the longitudinal plane 1

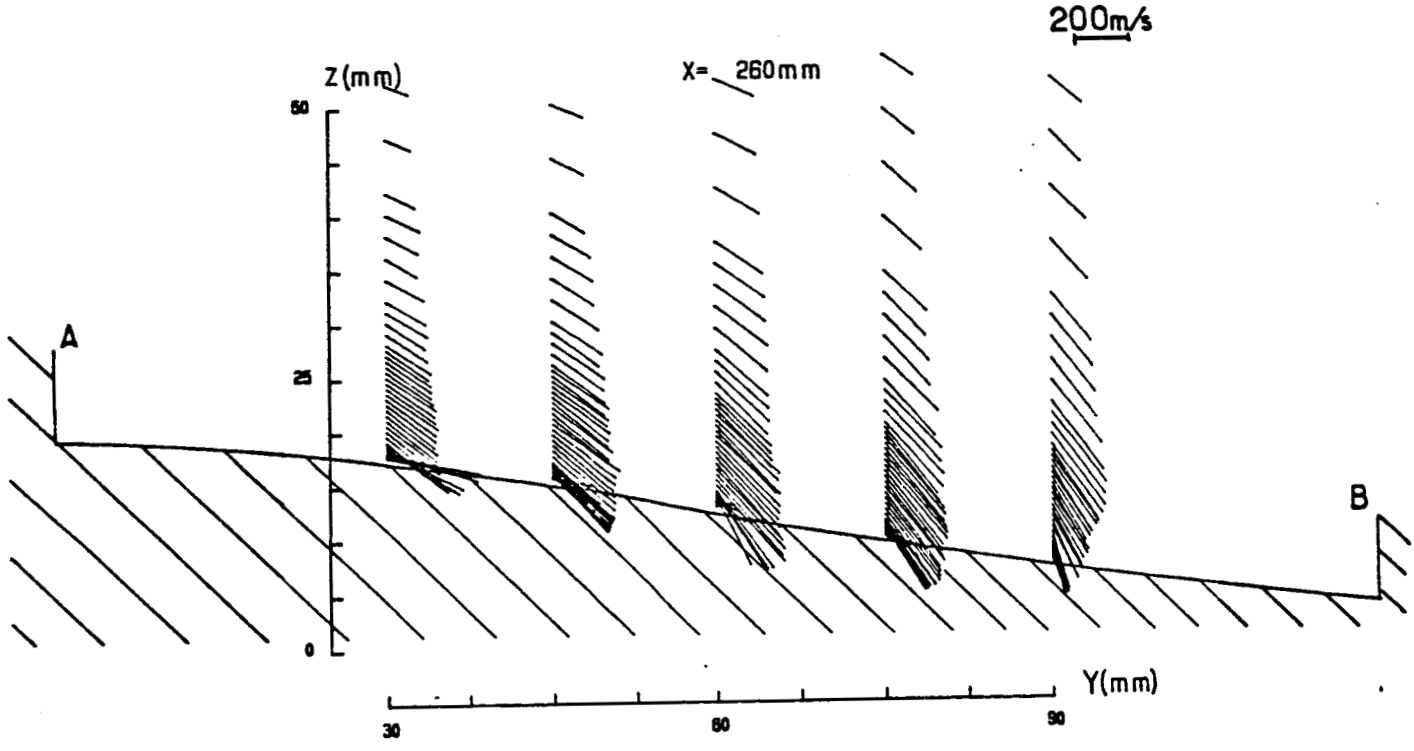

Figure 14: Projection of the velocity vectors in the transverse plane 6

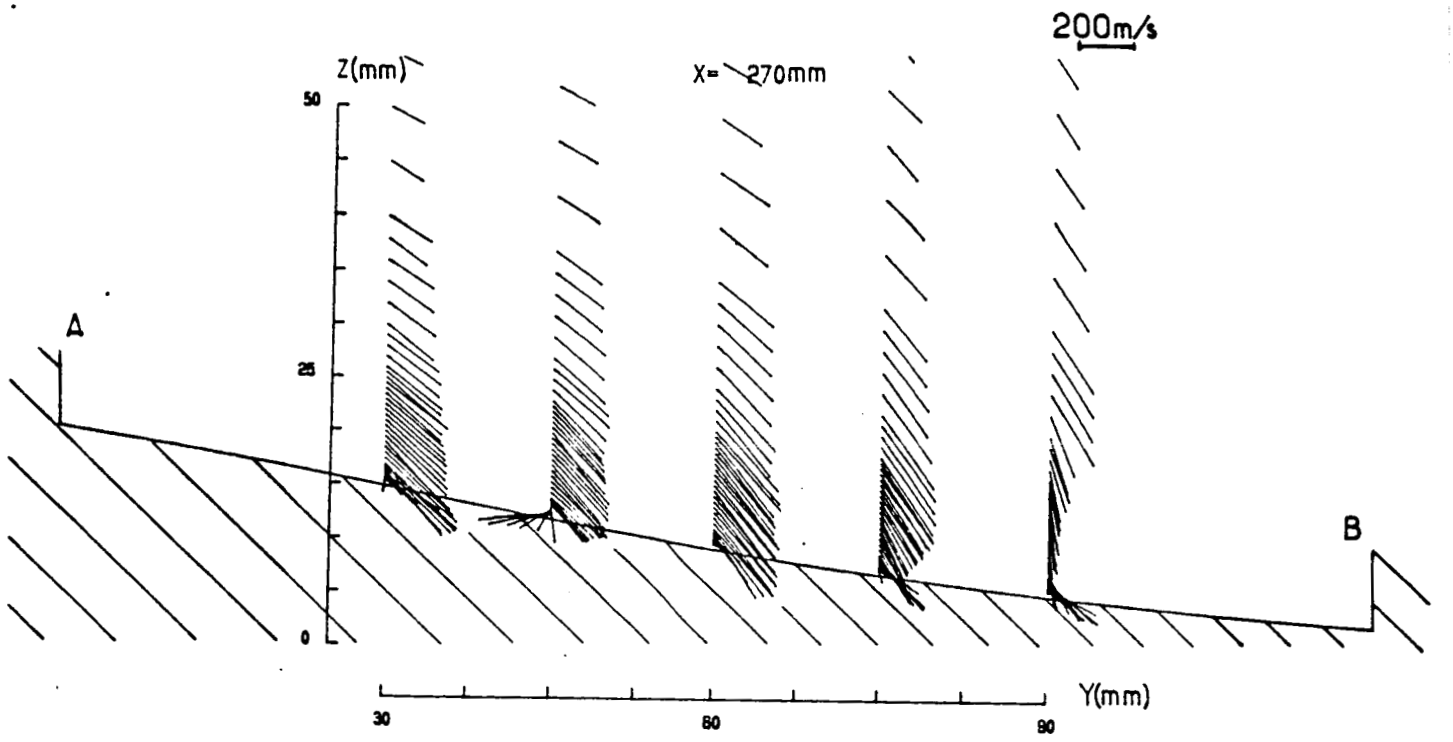

Figure 15: Projection of the velocity vectors in the transverse plane 7

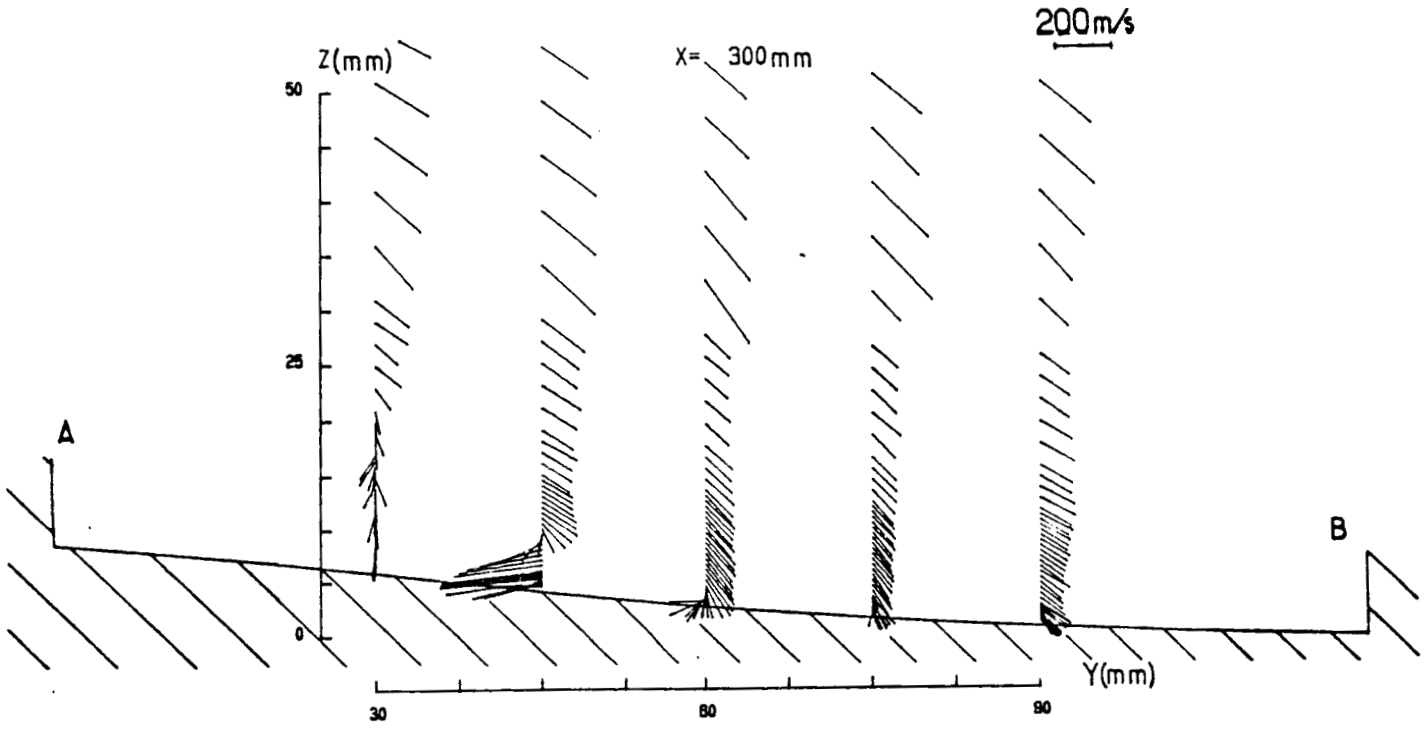

Figure 16: Projection of the velocity vectors in the transverse plane 8

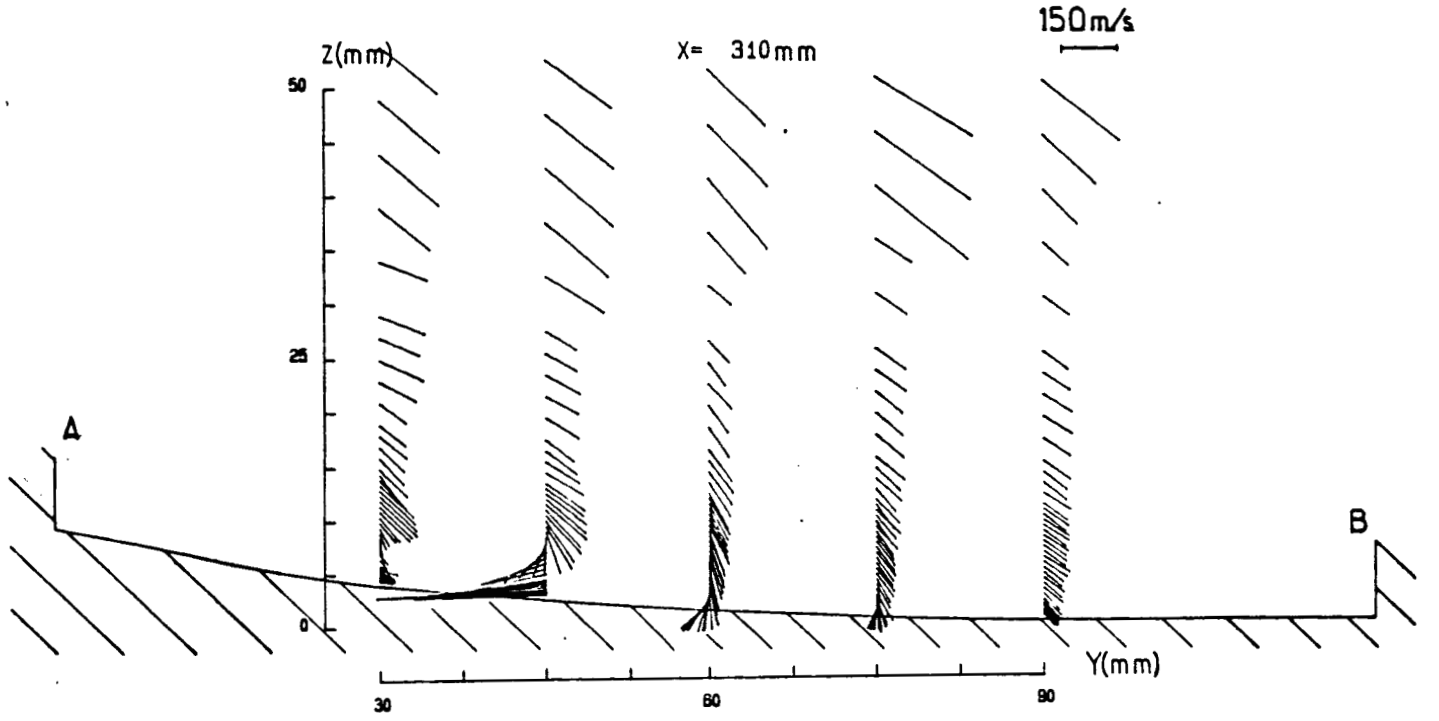

Figure 17: Projection of the velocity vectors in the transverse plane 9

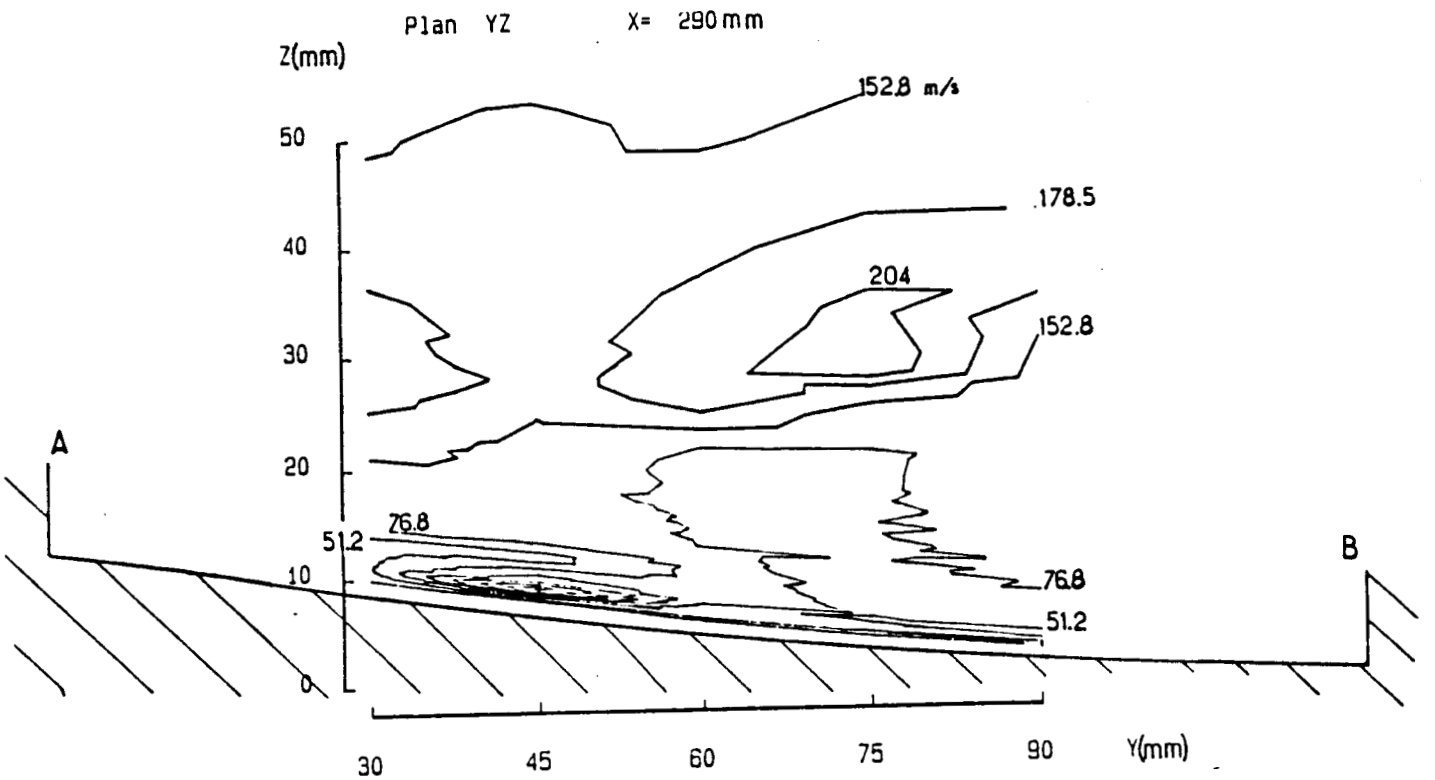

Figure 18: Lines of constant velocity module in a transverse plane

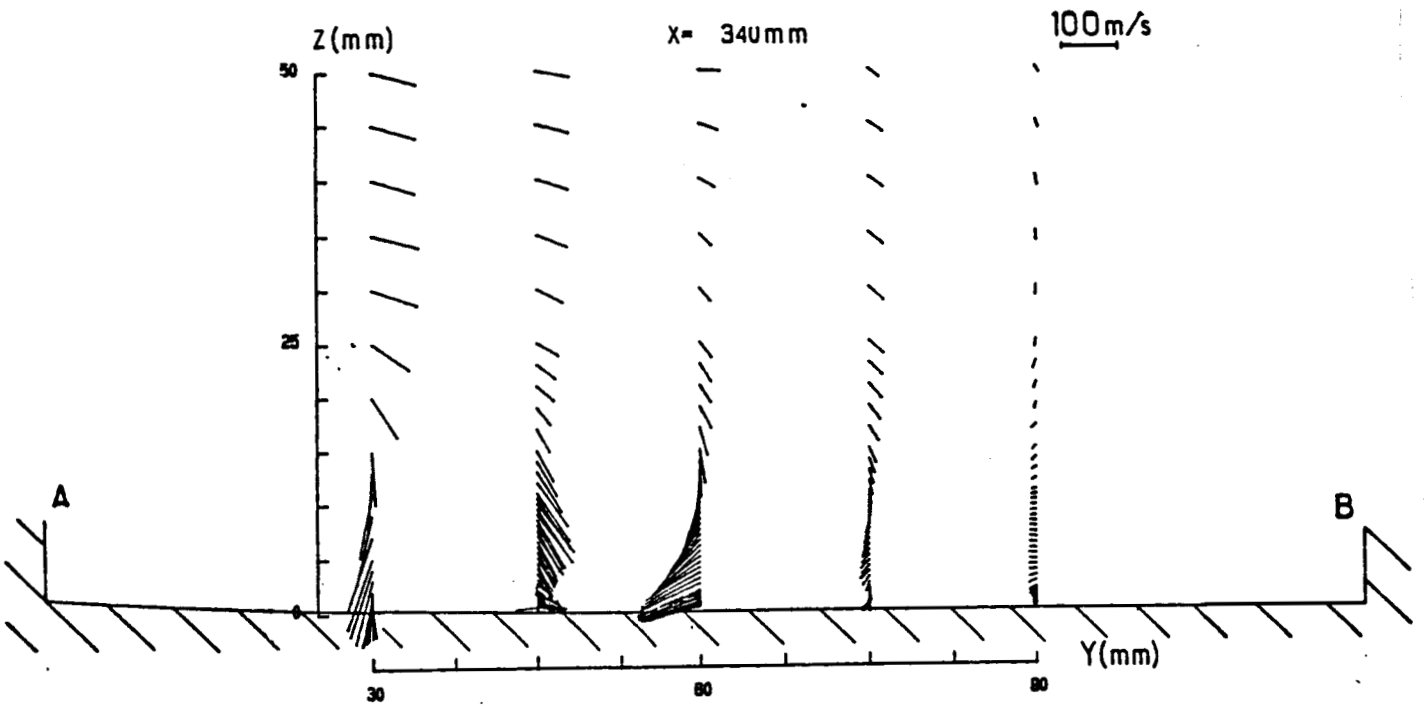

Figure 19: Projection of the velocity vectors in the transverse plane 11

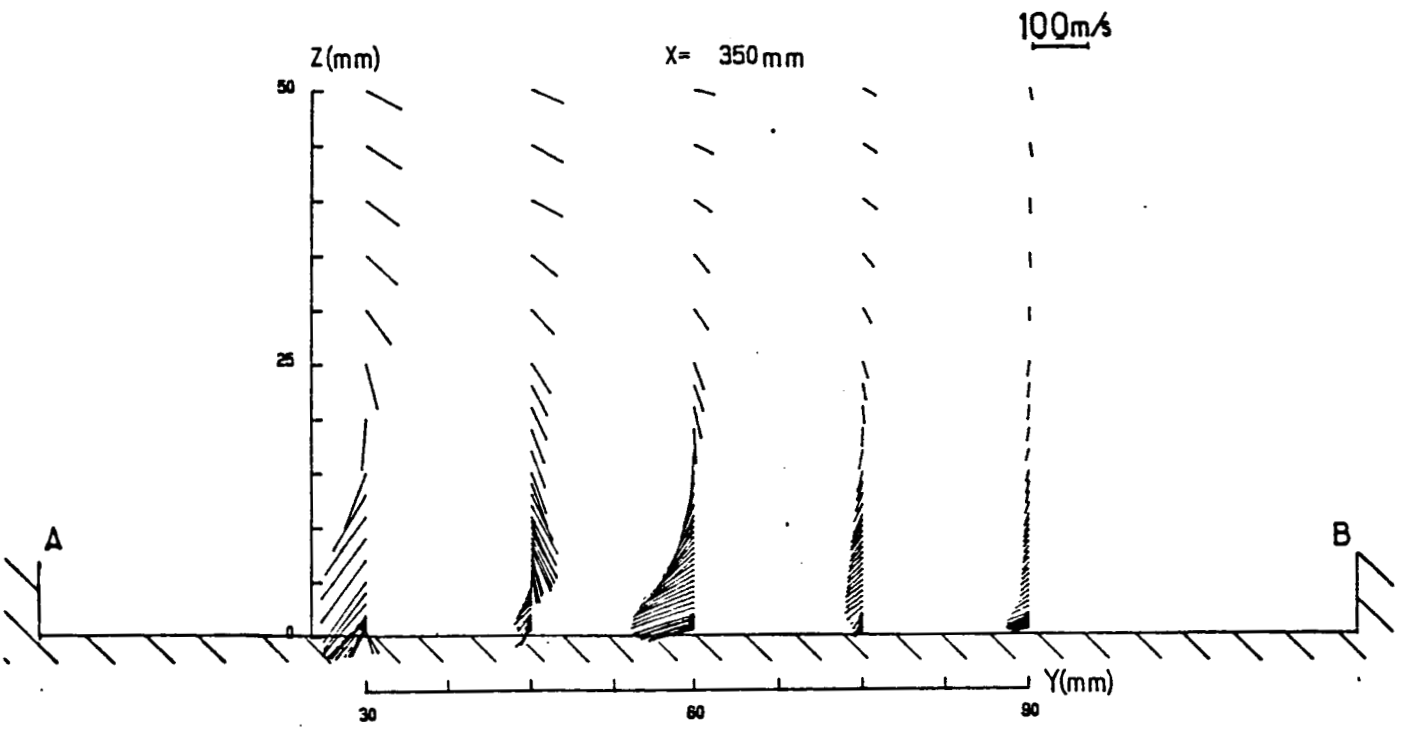

Figure 20: Projection of the velocity vectors in the transverse plane 12

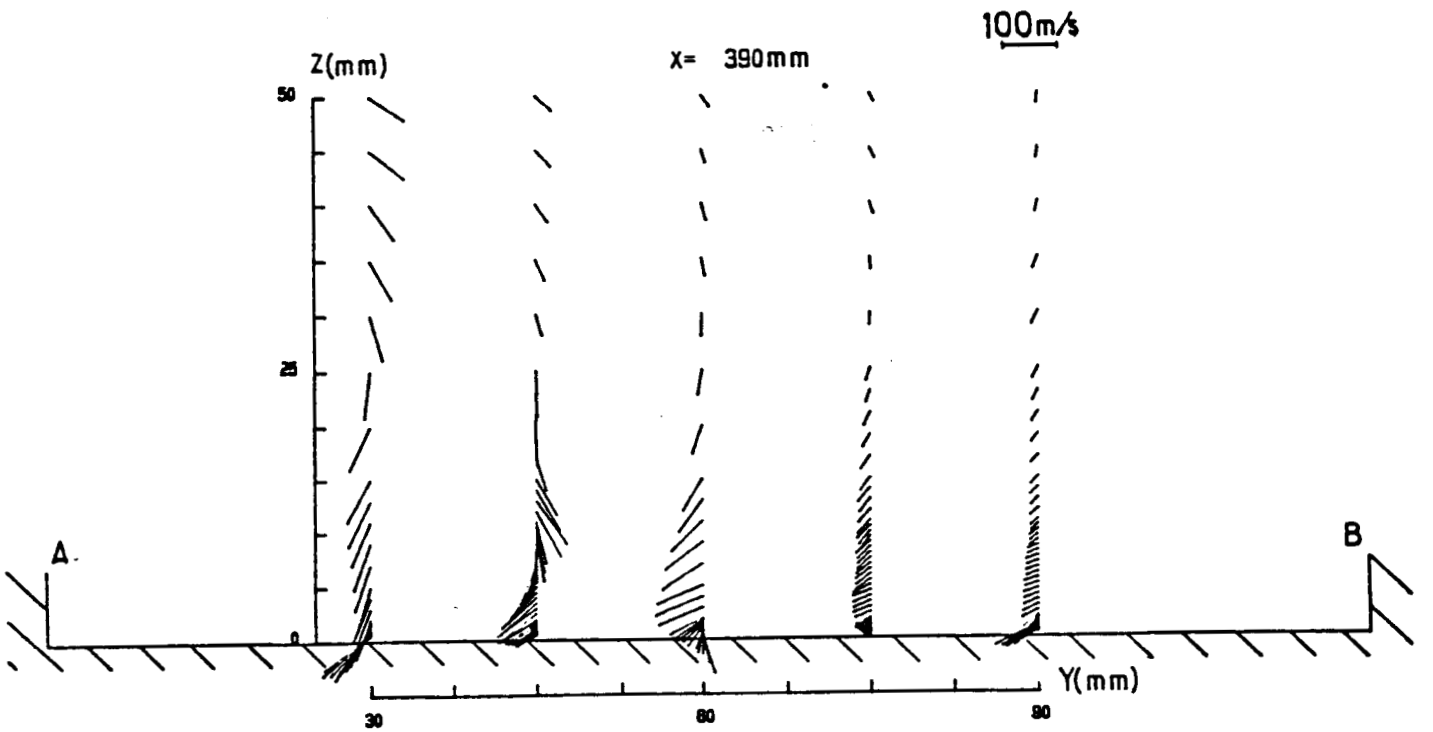

Figure 21: Projection of the velocity vectors in the transverse plane 13